The Effects of Mesoscale Eddies on the Stratification and Transport of an Ocean with a Circumpolar Channel

CARA C. HENNING AND GEOFFREY K. VALLIS

Geophysical Fluid Dynamics Laboratory, Princeton University, Princeton, New Jersey

(Manuscript received 21 May 2004, in final form 18 October 2004)

ABSTRACT

The effects of eddies in a primitive equation ocean model configured in a single hemisphere domain with circumpolar channels at their poleward ends are investigated; in particular, two regimes for the mass balance in the channel are investigated. With small overlying winds, the channel stratification is largely set by diffusion operating in the gyre portion of the domain: the depth scale varies with a fractional power of the diffusivity but has little dependence on the wind stress. As the winds are increased, the depth becomes increasingly controlled by a tendency toward small residual circulation. In this limit, a scaling theory is derived for the stratification in the channel that predicts the overall depth of the thermocline as a power of the wind stress and that allows the eddy length scale to differ from the channel length scale. The predicted depth depends on the details of the closure chosen for the eddy buoyancy flux, but in general it varies as some fractional power of the wind stress, and a channel-only numerical simulation agrees well with this prediction. When a gyre region is added to the channel, vertical diffusion in the gyre exerts some control on the channel stratification even at higher winds, forcing the mass balance into a mixed regime in which both eddy and diffusive effects are important. The depth scale varies less with the wind stress than in a channel-only configuration, and the residual mean circulation in the channel is maintained by the convergence of cross-isopycnal eddy buoyancy fluxes.

1. Introduction

Understanding the stratification of the ocean is a classical problem in physical oceanography. Much attention has focused, naturally enough, on the subtropical gyre and an ocean devoid of baroclinic eddies, and a reasonable understanding of that problem has emerged (Welander 1959; Stommel and Webster 1962; Samelson and Vallis 1997; and others). If, and realistically, baroclinic eddies are allowed to form, the problem becomes more difficult because it becomes dependent on understanding the transport properties of the baroclinic eddies, itself at least in part a problem in geostrophic turbulence. Nevertheless, although mesoscale eddies undoubtedly do affect the structure of the western boundary current and the subtropical thermocline (Radko and Marshall 2004), the basic structure suggested by Samelson and Vallis (1997)—that is, an upper-ventilated thermocline with a diffusive base—is still recognizable. The main difference, found by Henning and Vallis (2004), is that the dynamical balance in the base of the thermocline involves mesoscale eddies, as well as diffusion and mean advection, and its mean thickness does not appear to collapse to zero in the zero diapycnal diffusion limit. Even though the eddy kinetic energy is an order of magnitude larger than the mean kinetic energy, the eddies do not wholly dominate the thermocline structure.

However, this picture does not necessarily hold over the rest of the ocean, and in particular, in the Antarctic Circumpolar Channel (ACC), which remains unblocked by topography down to a depth of about 2500 m. Such a channel can have no net mean geostrophic meridional flow, since the longitudinal integral of the longitudinal pressure gradient is zero. In an ocean without eddies this leads to the formation of near vertical isopycnals in the channel (Vallis 2000), which are highly baroclinically unstable. It therefore is possible that the eddies would play a *leading-order* role in setting the channel stratification and hence (via thermal wind) the zonal transport in the channel.

Making various assumptions about the behavior of eddies, a number of investigators have suggested ways in which the transport of the ACC might then depend on wind stress (e.g., Johnson and Bryden 1989; Straub 1993; Marshall et al. 1993). These particular studies are all based at least partially on quasigeostrophic dynamics, which do not allow the stratification to change with the wind stress and which may not be valid for the ACC

Corresponding author address: Dr. Cara C. Henning, 395 McCone Hall, #4767, University of California, Berkeley, Berkeley, CA 94720.
E-mail: henning@atmos.berkeley.edu

© 2005 American Meteorological Society

(Killworth and Nanneh 1994). In the Fine Resolution Antarctic Model (FRAM) of the ACC, Doos and Webb (1994) showed that the diabatic circulation largely disappears when eddies are included, owing to a partial cancellation between the mean and eddy circulation. More recently, several studies have emerged that derive solutions for the channel thermocline depth under the assumption that this residual circulation should be close to zero. Karsten et al. (2002) find a scaling dependence on the wind stress to the first power and Marshall and Radko (2003) derive a solution for the stratification using the method of characteristics under this assumption. These studies both prescribe the surface buoyancy flux, while Gallego et al. (2004) underscores the importance of allowing the surface fluxes to adjust to the flow patterns (e.g., by using a restoring scheme), and they show that when the interior diabatic fluxes are small, the residual flow and surface buoyancy fluxes are necessarily weak. These studies have found success in idealized model simulations based on weak residual mean flow, but analysis of notoriously sparse data in the ACC is less conclusive. Karsten and Marshall (2002) found that while the eddy and mean circulations do tend to oppose each other in the observations, the residual mean flow can remain a third to a half the magnitude of the mean circulation, suggesting the zero-residual-mean condition may not be wholly appropriate in the real ocean.

The above evidently give conflicting evidence about the exact dependence of the transport and stratification on the wind stress, although their results underscore the importance of considering a realistic surface thermodynamic forcing and on resolving (or at least permitting) eddies if any progress on the question is to be made. In addition, all of these studies focus on a channel-only domain; because the channel isopycnals must connect smoothly with those of the subtropical gyre, it is possible that the channel stratification may be affected by the presence of the gyre and vice versa (as in Vallis 2000), and these considerations have motivated the present study. In particular, we explore the stratification and transport properties of a simply configured primitive equation model with a re-entrant, circumpolar channel adjacent to a subtropical gyre, as a simple model of the Southern Ocean. The simple geometry allows reasonably high horizontal resolution and extended integration periods to be achieved with a reasonable (but not comprehensive) range of parameters. Both thermodynamic and wind forcing are included. The numerical simulations are complemented by various theoretical arguments involving simply eddy closures and transformed Eulerian mean and residual mean diagnostics.

In section 2, we describe the model configuration. In section 3, we examine the qualitative structure of the eddy-permitting base case. We look at the stratification structure, the overturning circulation, and the buoyancy equation balance, and we see that the diapycnal circulation is balanced by explicit vertical diffusion in the gyre but by a small diapycnal eddy flux convergence in the channel. In section 4, we investigate two regimes that control how the stratification depth and transport vary with the wind stress and diffusion, one in which the residual mean transport tends toward zero and holds for higher winds, and one in which the depth scale is largely set by diffusion in the gyre and holds for lower winds. In section 5, we analyze the model results and find that gyre processes affect the channel stratification for all wind values. In section 6 we present a summary and discussion of the results.

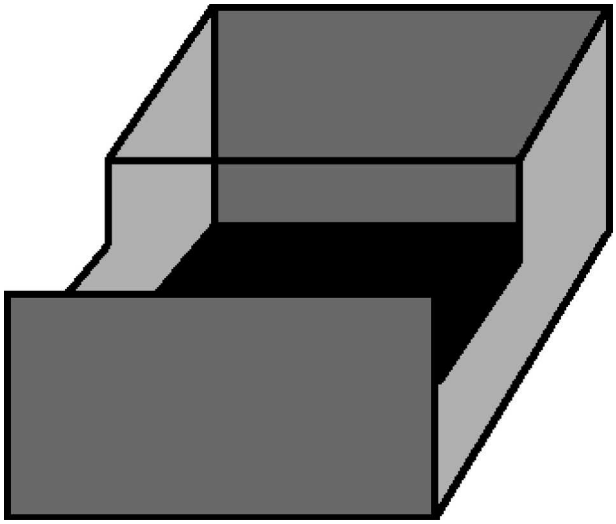

FIG. 1. A schematic drawing showing the domain used in this modeling study. The domain is a box with a channel at the poleward end. The channel is subject to a periodic boundary condition and represents the Antarctic Circumpolar Current in this simple geometry.

2. Model configuration

We use the Modular Ocean Model, version 3, (MOM3; Pacanowski and Griffies 1999) primitive equation model in an idealized configuration, shown schematically in Fig. 1. The domain is from 52° to 8°S and is 24° in longitude. At the surface, the vertical resolution is 35 m, stretching to 75 m at 600-m depth and 260 m at 4300-m depth (the domain bottom), giving a total of 31 vertical layers. A channel with a periodic boundary condition is present at the poleward end from latitudes 40° to 52°S. In one base case, this channel is left unblocked to any topography; in a second case, the channel is blocked at the first and last grid point in the logitudinal direction for all latitudes in the channel by a ridge that rises 2000 m high, leaving 2300 m unblocked. In the remainder of the paper, we will refer to the channel region and also to the remainder of the domain, which we will call the "gyre region."

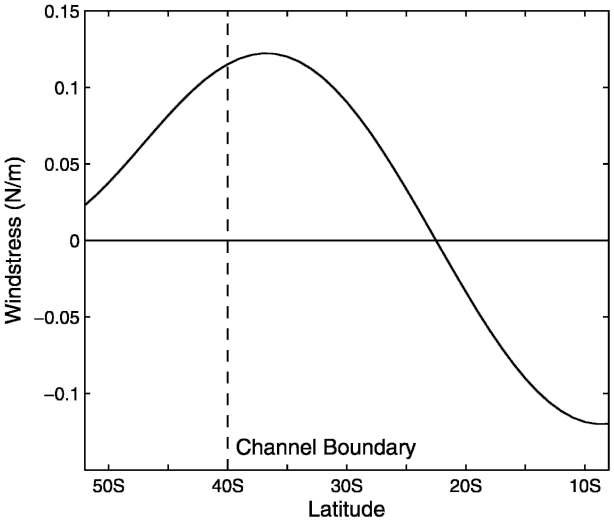

FIG. 2. Standard wind stress used in the base case. The wind stress curl has a maximum near 23°S.

The wind stress pattern is given in Fig. 2 so that the wind stress curl changes sign near 35°S. This leaves a rather small subpolar gyre between 35°S and the channel boundary. Temperature is the only active tracer and the surface temperature is restored to a linear profile that varies only in the latitudinal direction with a restoring time scale of 35 days, so that the net heat input is 50 W m^{-2} $°C^{-1}$.

Integrations were first performed with a relatively low-resolution grid with a latitudinal grid spacing of 2° and a variable longitudinal resolution such that the grid cells were everywhere almost square (we refer to this as a 2° grid). These cases were integrated with the smallest Laplacian horizontal diffusivity that maintained stability (50 m^2 s^{-1}). This is about an order of magnitude smaller than the diffusivity typically used to mimic eddy mixing and no Gent–McWilliams eddy parameterization scheme (Gent et al. 1995) was used so that these runs can be considered "noneddying." In general, the resulting horizontal diffusion term is much smaller than the vertical diffusion term in the tracer equation, so that there is little horizontal diapycnal diffusion associated with the sloping isopycnals away from the western boundary current. This low-resolution run was integrated for approximately 10 000 yr to reach equilibrium and was then interpolated onto a ¼° grid and the integration continued. In this case, vigorous eddies form in the channel and in the western boundary region. The subgrid-scale closure for momentum is a biharmonic scheme with coefficient $A_h = 1 \times 10^{18}$ m^4 s^{-1}. For temperature, we use the Gent–McWilliams scheme, but with a very small coefficient $\kappa_{GM} = 8 \times 10^{-1}$ m^2 s^{-1}. This parameterization removes power at the grid scale without the large diapycnal mixing associated with a conventional horizontal mixing scheme. However, the coefficient is small and does not significantly affect the buoyancy budget.

The two eddying base cases were run for over 1700 yr (see Table 1). In general, the upper-ocean equilibrated first, with the deeper ocean equilibrating more slowly. We found that equilibration was largely accomplished after this period, although there is still a very small tendency in the abyssal ocean in the case without topography. We also ran several different wind strengths and diffusivities for the base case that included the topographic ridge. These were started either after 600 yr of the base case or from their own low-resolution spinup case. In general, the cases started from the equilibrated runs took around 100–200 yr to re-equilibrate the upper 1500 m.

3. Eddying base case—A qualitative overview

Estimating the first baroclinic radius of deformation as *NH/f* and using $H = 1500$ m gives a radius of deformation of 35 km at 45°S in the center of the channel. At this latitude, the model resolution is 20 km, suggesting that the first radius of deformation is just resolved in the channel. Typically, baroclinic eddies have a scale of a few times the deformation radius, both because the fastest growing eddy typically has a length scale of a few times the deformation radius (4 times in the Eady problem) and because of the nonlinear cascade to larger scales, so our resolution should be sufficient to permit eddy formation.

Figure 3 shows the eddy kinetic energy at the surface averaged around the channel. Using *Geosat* altimeter data the average eddy kinetic energy in the ACC between 30° and 60°S is 0.0159 m^2 s^{-2}, with locally large values of 0.1 m^2 s^{-2} in Drake Passage and 0.3 m^2 s^{-2} in the Agulhas Current region (Wilkin and Morrow 1994). In our model, the eddy kinetic energy is largest near the channel boundary, is still significant at 45°S, but then diminishes south of this latitude. The average value in the channel is 0.0224 m^2 s^{-2}, suggesting a root-mean-squared velocity of 0.150 m s^{-1}. Evidently, the eddy ki-

TABLE 1. A summary of the experiments run with varying winds. The eddying case is started from a low-resolution spinup run for 10 000 yr or from the final state of another eddying run as noted.

	With ridge	Initial condition	Length of eddy simulation (yr)
No wind	Yes	Winds × 0.2 case	80
Wind × 0.2	Yes	Winds × 0.75 case	100
Wind × 0.75	Yes	Low-resolution spinup	390
Base case	No	Low-resolution spinup	1745
Base case	Yes	Low-resolution spinup	1835
Wind × 1.5	Yes	Low-resolution spinup	425
Wind × 2	Yes	Winds × 3 case	70
Wind × 3	Yes	Winds × 1.5 case	160
Wind × 5	Yes	Winds × 3 case	105

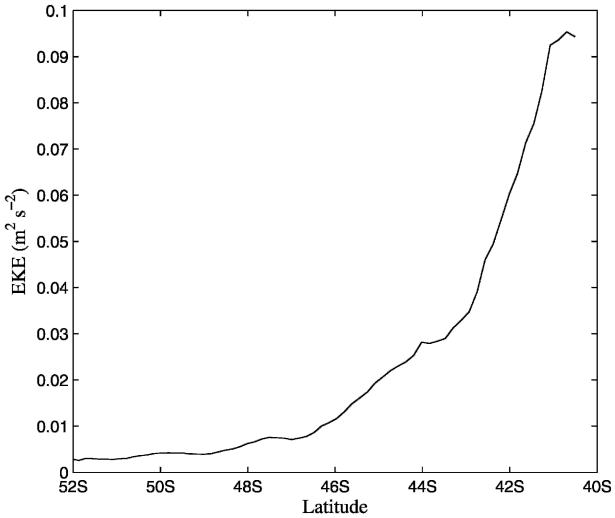

FIG. 3. The surface eddy kinetic energy averaged around the longitudes of the channel (m^2 s^{-2}).

netic energy is sufficiently large to be of the same order as the real ocean in the circumpolar current.

a. Density structure

Figure 4 shows the potential temperature (here, equivalent to density) sections for the low-resolution and eddying cases both with and without the topographic ridge. In the low-resolution case without topography, the coldest water is largely trapped in the channel similar to Vallis (2000). When the ridge is added, deep stratification forms beneath the level of the ridge. In the eddying cases, the two cases are less easily distinguished. In the case with topography, eddies have formed as a result of baroclinic instability and have eroded away the available potential energy (APE) associated with steeply sloping isotherms until the isotherms are nearly parallel within the channel. The stratification is above the topography so that none of the outcropping layers are blocked by topography. The case without topography looks similar to the topography case; the main differences are the deep 4°C water (which we find continues to rise slowly as the model is integrated further) and the slope of the isotherms in the channel. The latter tends to be somewhat steeper than the corresponding topography case slope. Thus, rather unlike the non-eddying model in Vallis (2000), the presence of topography in our eddying model does not immediately lead to deep stratification and the abyss fills with the coldest water available at the surface.

b. Overturning circulation

To understand how the eddies help to maintain the thermal structure shown in Fig. 4, we examine the residual overturning stream function for the eddy-permitting case. To do so, we calculate the streamfunction along density surfaces,

$$\psi_\sigma = \int_{\text{channel}} \int_{z=-H(\phi)}^{z[\phi,\lambda,\rho(\phi,\lambda,t)]} v(\phi, \lambda, z', t) R \cos(\lambda)\, dz'\, d\phi, \tag{1}$$

where λ is the longitude, ϕ is the latitude, $z = -H(\phi)$ is the ocean floor, and $z(\phi, \theta, \rho)$ is the depth of an isopycnal (e.g., Doos and Webb 1994). Here, the streamfunction is the integral of the instantaneous velocity in longitude and from the bottom to the depth of a given instantaneous density surface. (This representation is to be compared with the usual mean overturning streamfunction in which the time-mean velocity is integrated up to constant depths rather than constant density surfaces.) The residual mean is then obtained by time averaging many such snapshots and mapping back to depth coordinates using the time-averaged depth of each isopycnal. McIntosh and McDougall (1996) have shown that the above representation is equivalent, to leading order in the perturbation amplitude, to the residual circulation calculated in depth coordinates, using the "transformed Eulerian mean" formulation of Andrews and McIntyre (1978). Figure 5 shows the mean streamfunction (upper), the eddy streamfunction (middle), and the residual mean streamfunction (lower) for the case with topography, where the mean (velocity integrated to depth surfaces) and residual mean (velocity integrated to density surfaces) are calculated as explained above and the eddy streamfunction has been deduced as the difference between the two. The solid lines represent clockwise rotation and the dashed lines represent counterclockwise rotation. The time and longitudinally averaged isopycnals are also shown in the figure.

1) CHANNEL REGION

In the channel region, the mean equatorward Ekman flow out of the upper layer is returned near the level of the topography and then lifted at the poleward domain boundary. The eddy circulation is in the opposite direction, and the counterclockwise rotation releases the available potential energy stored in the stratification, consistent with baroclinic eddy formation. The residual mean streamfunction, as the sum of two opposing circulations, is smaller in magnitude than either the eddy or mean streamfunctions, with the average ratio of residual to mean equal to 0.5 in the core of the circulation (near 500-m depth and 42°S). The residual is poleward at the surface, in accordance with a surface buoyancy flux from the ocean to the atmosphere in the channel (not shown), and equatorward at depth. This residual mean circulation must be balanced locally by a diabatic process, either background diffusion or an explicitly diapycnal eddy term. To determine which, Fig. 6 shows the buoyancy equation terms near the channel bound-

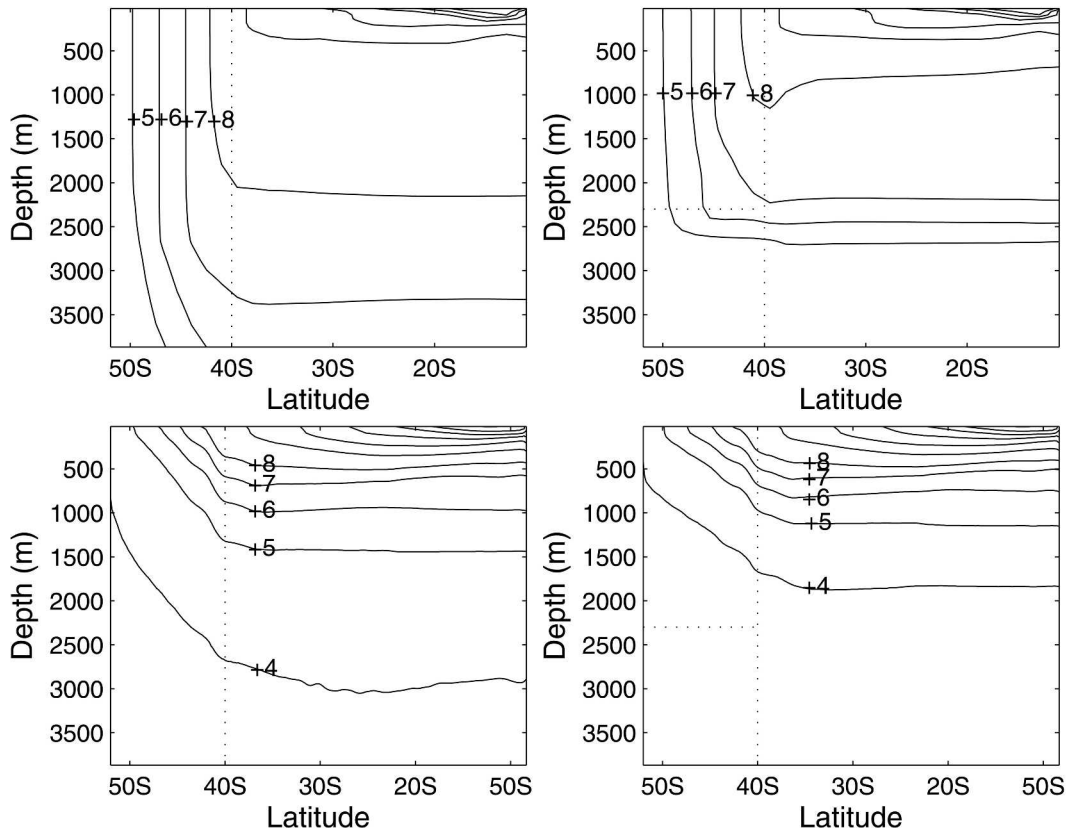

FIG. 4. Potential temperature section for the low-resolution case (top left) without topography and (top right) with topography for the eddy-permitting case (bottom left) without topography and (bottom right) with topography. The topography is a ridge that partially blocks the channel, and the height is shown as a dotted line. The channel boundary is also shown with a dotted line. The temperature sections are all averaged from 9° to 13°E in the center of the domain. The contour interval is 1°C in the channel and 2°C elsewhere.

ary (averaged from 39° to 41°S) for the eddy-permitting case (left) and eddy-permitting case in the transformed Eulerian mean (TEM) form (right). Here, the eddy quantities are the deviation from the time and longitudinally averaged quantities, so that the eddies contain the contribution from the transient and standing eddies. The buoyancy equation in steady state is then

$$\bar{v}\bar{b}_y + \bar{w}\bar{b}_z = -(\overline{v'b'})_y - (\overline{w'b'})_z + \kappa_v b_{zz} \tag{2}$$

for the eddying case and

$$(\bar{v} + v^*)\bar{b}_y + (\bar{w} + w^*)\bar{b}_z = -G_z + \kappa_v b_{zz} \tag{3}$$

for the TEM form of the eddying case, where

$$(v^*, w^*) = \left[-\left(\frac{\overline{v'b'}}{b_z}\right)_z, \left(\frac{\overline{v'b'}}{b_z}\right)_y \right] \tag{4}$$

is a two-dimensional "eddy-induced velocity" and

$$G = \frac{\overline{\mathbf{v}'b'} \cdot \nabla\bar{b}}{\partial\bar{b}/\partial z}, \tag{5}$$

and the reader can then verify that

$$G_z + v^* \cdot \nabla b \equiv \nabla \cdot \overline{v'b'}. \tag{6}$$

Here, G_z captures the contribution to the eddy flux convergence from the cross-isopycnal eddy fluxes and $v^*\bar{b} + w^*\bar{b}_z$ captures the contribution from the along-isopycnal eddy fluxes. Figure 6 shows the balance of terms in the buoyancy equation in the channel region near the boundary in terms of the eddy convergences (left) and also in the TEM form (right). In this boundary away from the surface, the mean vertical advection is balanced almost entirely by the eddy flux convergences, so that in the TEM formulation, the along-isopycnal flux convergence, $v^*b_y + w^*\bar{b}_z$ primarily balances the mean vertical advection, $\bar{w}\bar{b}_z$. Further analysis reveals that the dominant eddy advection term is $w^*\bar{b}_z$ and the residual advection is largely $(\bar{w} + w^*)\bar{b}_z \sim 0$. To the extent that this residual is not zero it is balanced locally by the G_z term. The explicit diffusion term is small and not discernible on the figure. Note that the eddies have created uniformly spaced isopycnals, presumably a consequence of their tendency to

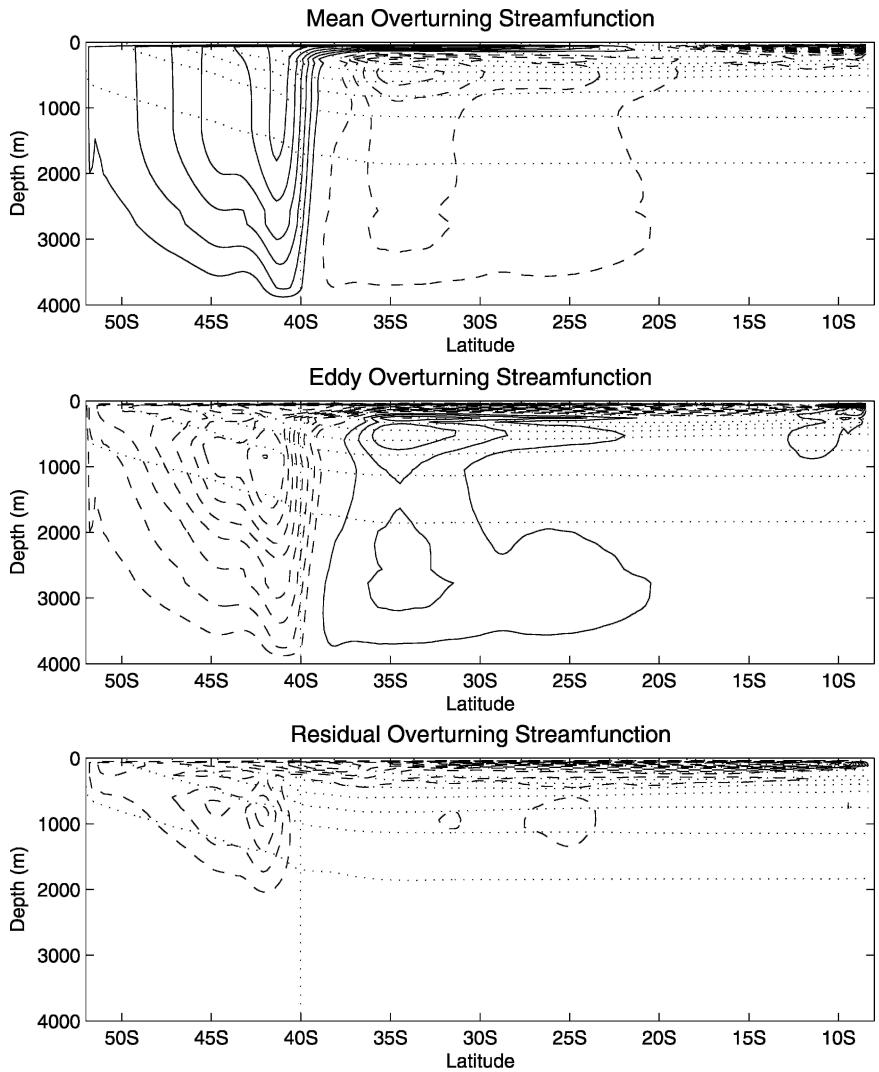

FIG. 5. (top) Mean, (middle) eddy, and (bottom) residual mean overturning streamfunction for the base case with topography. The mean circulation is found by integrating the mean velocity down to constant depth surfaces, and the residual is found by integrating down to density surfaces, with the eddy being the difference between the two. The solid lines indicate clockwise rotation, and the dashed lines indicate counterclockwise rotation. The contour interval is 0.25 Sv (1 Sv $\equiv 10^6$ m^3 s^{-1}). Also shown are the time-averaged isothermals, with a contour interval of 1°C (from 4° to 18°C). The channel boundary is near 40°S.

homogenize potential vorticity or thickness, which are very similar if the effects of β are small. In such a region, Laplacian diffusion is necessarily small. Thus, in this region the residual flow is balanced by the cross-isopycnal eddy flux convergence and not by explicit vertical diffusion,

$$(\overline{w} + w^*)\overline{b}_z \approx G_z. \tag{7}$$

This balance was also found in a wind-forced channel model by Gille and Davis (1999).

2) GYRE REGION

Figure 7 shows the buoyancy equation terms in the gyre portion of the case with the topographic ridge, where now the average is only in time and the eddy quantities include only the transient eddies. The terms are averaged from longitude 6–8 and from 25° to 15°S. Here, the residual circulation is small and crosses isopycnals down to 400 m in the internal thermocline region. Along isopycnals that outcrop in the channel, the circulation tends to be small but does appear to cross isopycnals, especially near 25°S where the wind stress curl is at a maximum. Any net residual circulation into the thermocline will have to be balanced by a diapycnal process.

The balance between 500 and 1500 m, or the location of the isotherms that outcrop in the channel, is largely between the upwelling advection and the eddy terms,

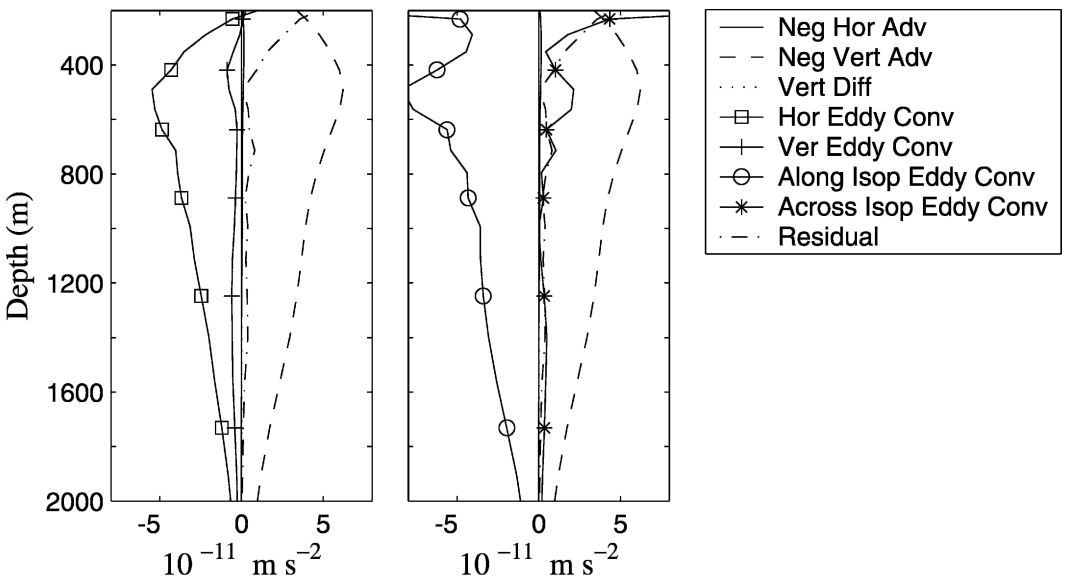

FIG. 6. The buoyancy equation terms in the channel boundary region of (left) eddy-permitting case and (right) eddy-permitting case in the transformed Eulerian mean form. The terms are calculated using mean variables that have been averaged in longitude and time so that the eddy terms include both the transient and standing eddy contributions. The terms: negative horizontal advection ($-\overline{v}\overline{b}_y$), negative vertical advection ($-\overline{w}\overline{b}_z$), vertical diffusion ($\kappa_v\overline{b}_{zz}$), horizontal eddy convergence [$-(\overline{v'b'})_y$], vertical eddy convergence [$-(\overline{w'b'}_z)$], along-isopycnal eddy convergence ($-v^*\overline{b}_y - w^*\overline{b}_z$), cross-isopycnal eddy convergence ($-G_z$), and the residual, or the sum of the above terms. The residual contains contributions from the time tendency, the convection, and any numerical errors.

with any difference being balanced by the diffusion. In this region, G_z is small and the diapycnal flux is accomplished by the explicit diffusion. This balance is the same as we found in a similar eddy-permitting box only study (Henning and Vallis 2004), suggesting the gyre dynamics are not strongly affected by the presence of a channel.

4. Scaling theory for stratification and transport

We now consider the variation of the density structure and transport with the diffusivity and wind stress. We begin with a conceptual picture of how the circulation can vary with the wind stress and examine two limits in the case of varying winds. As pointed out by Gnanadesikan and Hallberg (2000), the mass balance in a two-layer channel can be closed in two ways. The wind stress drives an equatorward flow out of the channel in the upper layer and geostrophic return flow in the lower layer. To close this circulation, the eddies can drive a poleward mass flux in the upper layer equal in magnitude to the Ekman flux and an equal but opposite eddy mass flux in the lower layer. In this case, there is no net mass flux in either layer and the residual mean circulation is zero, as summarized in Fig. 8 (left-hand side). Alternatively, there can be a direct diapycnal mass flux from the lower layer to the upper layer near the poleward boundary to close the circulation. In this latter case, there will be a net residual mean circulation and some diapycnal process will be necessary to sustain the circulation. This scenario is summarized in Fig. 8 (right-hand side).

In section 3b, we observed that in the base case, the residual circulation is smaller than the mean circulation in the channel. Previous studies (e.g., Johnson and Bryden 1989; Karsten et al. 2002) derive scaling theories by assuming the residual circulation is zero in the channel. This is not strictly true in our base case. However, Fig. 9 shows the ratio of the residual mean to the mean circulation for a variety of wind stresses in the model simulations (further details of these runs will be given in section 5). The abscissa shows the normalized wind stresses as compared with the base case wind stress. For winds lower than 0.75 times the base case, the relationship is not monotonic, suggesting these values lie in a different regime. However, as the winds are increased beyond this value, this ratio becomes very small with increasing winds, suggesting that the tendency toward zero residual mean circulation plays a role in setting the stratification for higher winds. However, at low winds, we will see that the gyre diffusion is responsible for setting the stratification, and not the zero-residual-mean condition. Thus, we proceed by assuming there are two regimes, a regime of low residual mean circulation at high winds, and a regime of a substantial, diffusively driven residual mean circulation at low winds. We will examine these two regimes separately, and then investigate the empirical scaling for varying winds within the model.

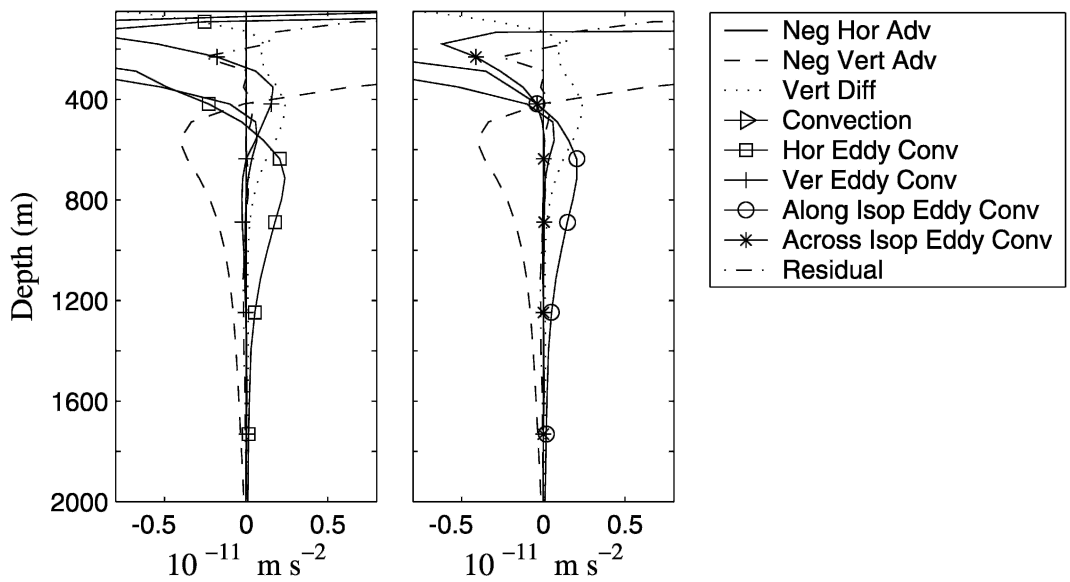

FIG. 7. The same as Fig. 6, but in the middle of the gyre portion of the model. The average is now only in time, and so the negative horizontal advection becomes $(-\overline{u}\overline{b}_x - \overline{v}\overline{b}_y)$ and the horizontal eddy flux convergence becomes $[-(\overline{u'b'})_x - (\overline{v'b'})_y]$. The terms are averaged away from the western boundary region, for longitudes 6–8 and from 25° to 16°S.

a. The zero-residual-circulation condition

To derive a depth scaling under the zero-residual-mean condition, we will proceed similarly to Karsten et al. (2002) by setting the mean Ekman streamfunction, given by $\overline{\psi} = \tau/(\rho_0 f) \equiv \tau_0/f$ equal to the eddy streamfunction, given by $\psi^* = (\overline{v'b'})/\overline{b}_z$, and assuming the eddy flux can be parameterized as a downgradient flux of buoyancy, $\overline{v'b'} \approx \kappa_e \overline{b}_y$. Taking the horizontal and vertical variation in the buoyancy to be the same, then

$$\psi^* \approx \frac{\kappa_e D}{L}, \tag{8}$$

where L is the channel width, D is the stratification depth, and κ_e is the eddy diffusivity. Equating $\overline{\psi}$ and ψ^* and solving for D yields

$$D \sim \frac{\tau_o L}{\kappa_e f}. \tag{9}$$

It remains to determine the eddy diffusivity κ_e, and in general this diffusivity will contain a dependence on the depth scale itself. We assume that this diffusivity can be parameterized as a root-mean-squared velocity multiplied by an eddy length scale,

$$\kappa_e \sim U_e L_e. \tag{10}$$

To proceed, we must prescribe a scaling for the eddy

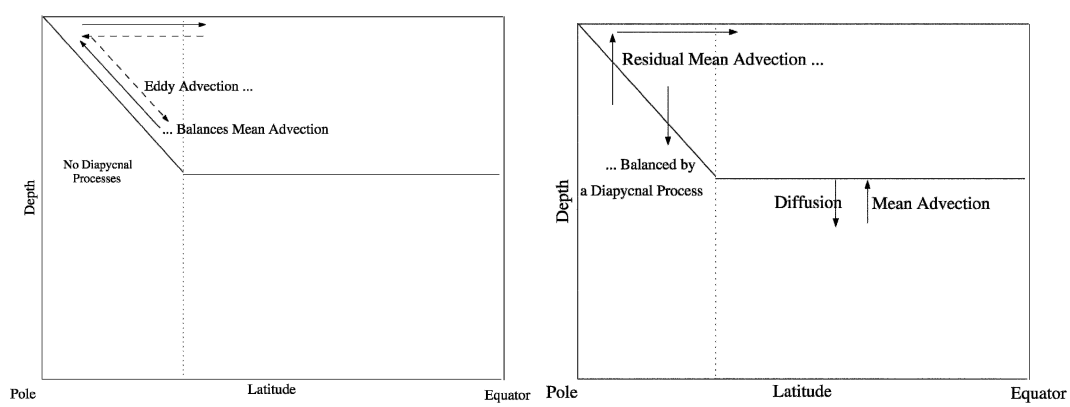

FIG. 8. A schematic diagram showing the assumption about the two regimes describing the circulation in the channel. The (left) first assumes that there is zero residual circulation in the channel, whereas the (right) second is a wholly thermodynamic balance in which a diapycnal process must balance a cross-isopycnal net mass flux.

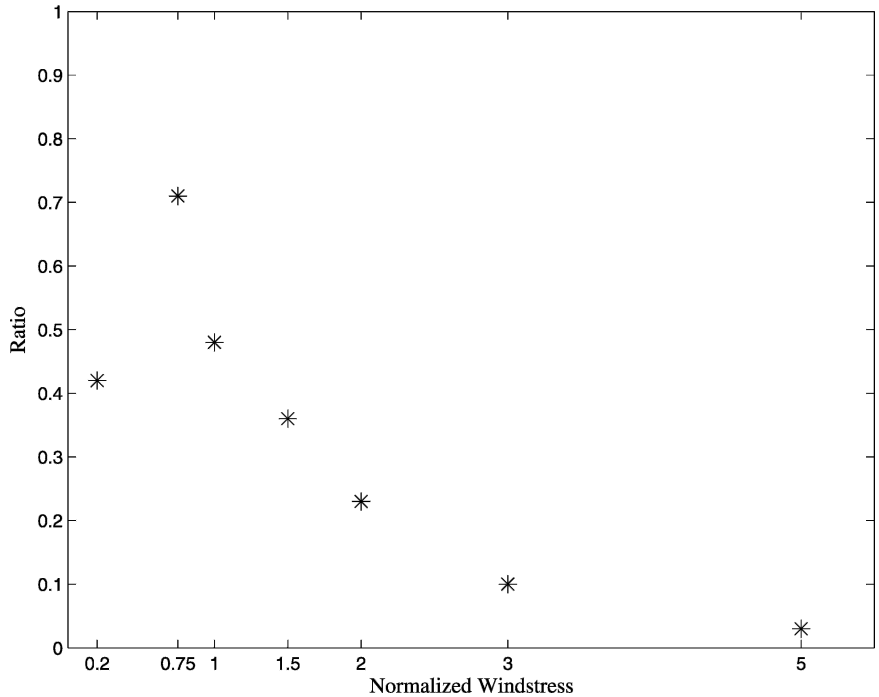

FIG. 9. The ratio of the residual mean circulation to the mean circulation at 500-m depth in the core of the circulation (42°S) for a variety of wind stress values. The x axis is the wind stress normalized by the base case wind stress.

velocity and length scales. Unlike Karsten et al. (2002), we will allow the eddy length scale to differ from the channel length scale and the eddy velocity scale to differ from the mean thermal wind scale. Following Larichev and Held (1995), we assume that the eddy energy will be equipartitioned between the kinetic energy and available potential energy, an assumption that links the eddy velocity and eddy length scale. Then,

$$\overline{v'^2} \sim \frac{\overline{b'^2}}{N^2}, \tag{11}$$

or

$$\overline{v'^2} \sim \frac{\overline{b}_y^2 L_e^2}{N^2}. \tag{12}$$

Using $N^2 \sim \Delta b/D$, and solving for U_e,

$$U_e \sim (\Delta b D)^{1/2} \frac{L_e}{L}, \tag{13}$$

or using (10),

$$\kappa_e \sim (\Delta b D)^{1/2} \frac{L_e^2}{L}, \tag{14}$$

so that given L_e, this gives the scaling for κ_e under the equipartition assumption.

Regarding the eddy length scale, eddies will tend to form near the radius of deformation, ND/f, and eddy kinetic energy will cascade upscale through nonlinear interactions. On the β plane, the cascade will be arrested near the Rhines scale, $L_{\mathrm{Rh}} \sim (U_e/\beta)$ (Rhines 1975; Vallis and Maltrud 1993). However, if the Rhines scale is larger than the channel width scale, then the cascade will proceed all the way to the channel scale. In our simulations the Rhines scale is typically smaller than the channel scale and the zonal current organizes in bands at about the Rhines scale (not shown). Taking this as the relevant length scale, then $(U_e/\beta)^{1/2} \sim (U_e a/f)^{1/2}$, where a is the radius of the earth. Then, using (14)

$$\kappa_e \sim \frac{(\Delta b D)^{3/2}}{f^2 L} \left(\frac{a}{L}\right)^2, \tag{15}$$

and using (9) gives finally

$$D \sim \left(\frac{\tau_o L^2 f}{\Delta b^{3/2}}\right)^{2/5} \left(\frac{L}{a}\right)^{4/5}, \tag{16}$$

where the details are given in the appendix.

The above ideas suggest that as the wind stress increases, the depth scale will increase until the eddy streamfunction can entirely balance the mean streamfunction and the residual streamfunction is zero. For this particular choice of eddy closure and eddy length scale, we predict the depth will vary as the wind stress to the 2/5 power. Alternatively, we might have assumed the length scale is either the deformation radius, which predicts that $D \sim \tau^{2/5}$ and differs from (16) only by the

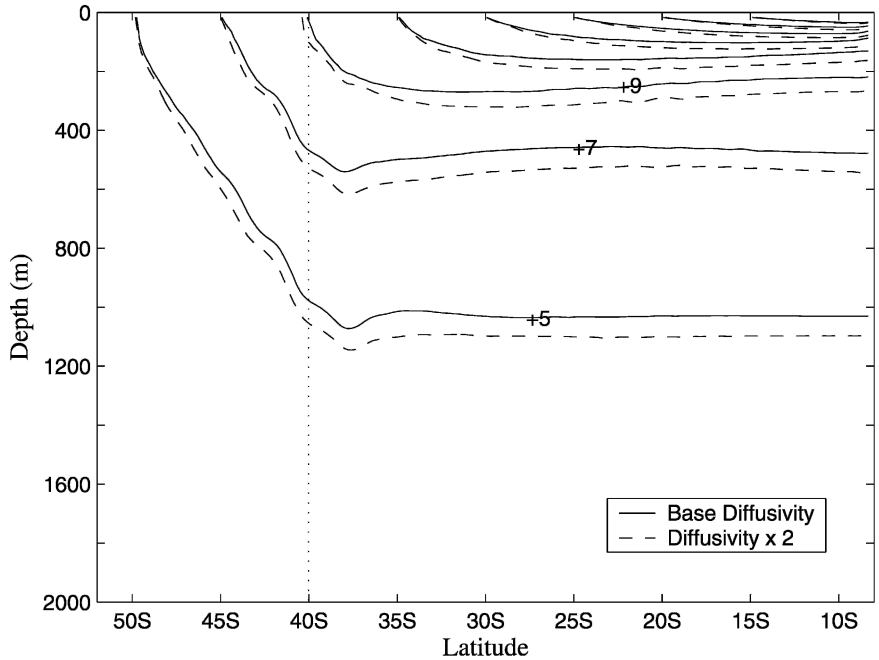

FIG. 10. A potential temperature section in the center of the domain for the case with no winds (and including topography). The solid lines are the case using the base diffusivity (2×10^{-5} m^2 s^{-1}), and the dashed lines use 2 times this diffusivity. The isotherms run from 5° to 20°C, with a contour interval of 2°C.

factor $(L/a)^{4/5}$, or the channel scale, which predicts $D \sim \tau^{2/3}$ under the equipartition assumption or $D \sim \tau^{1/2}$ if instead U_e is assumed to be given by the thermal wind equation (as in Karsten et al. 2002), where the details are given in the appendix. All of these predictions are slightly different but predict that the depth scale will vary with the wind stress, with the power dependence close to $\tau^{1/2}$.

b. Zero wind stress: The diffusive limit

In the other limit the mass flux is cross-isopycnal and is driven by a diapycnal process. Based on Fig. 9, we expect this limit may be more important for lower winds, where the residual mean remains a significant fraction of the mean. It is useful, then, to explore a case, which has no wind stress at all. In this case, there is no Ekman flux, but there is surface buoyancy forcing via a restoring term. This buoyancy forcing leads to eddies in the channel, since the no-net-meridional-flow condition creates steep isopycnals which become baroclinically unstable. However, these eddies are somewhat less vigorous than the eddies in the cases with winds. In the gyre, the buoyancy sources created by the forcing can be easily redistributed in the horizontal by meridional flow, there is no source of APE, and there is little eddy activity.

In the absence of diapycnal processes, the eddies will tend to reduce the stratification to a thin surface layer. However, if background vertical diffusion is present, it will tend to pull the warm surface water downward and deepen the stratification. Figure 10 shows the potential temperature section in the no-winds case near the center of the domain for the base diffusivity ($\kappa_v = 2 \times 10^{-5}$ m^2 s^{-1}, solid) and for a case with double the diffusivity (dashed). The cases are similar, and the tightest stratification is confined to within 200–300 m of the surface, with the coldest isotherms reaching down to about 1000 m, and the case with stronger diffusion has deeper stratification. Figure 11 shows the terms in the TEM form of the buoyancy equation in the eddy-permitting no-winds case with base diffusivity in the gyre (left) and channel (right). In the gyre, the vertical advection is balanced by the background diffusion, so that the diffusion is responsible for setting the stratification depth. On the other hand, in the channel, the vertical diffusion term is small. Here, the isotherms are more uniformly spaced so that Laplacian diffusion is necessarily ineffective. Instead, the stratification is maintained by the diapycnal eddy term, G_z, and not by the explicit diffusion.

However, the stratification in both the gyre and channel are consistent with a diffusive balance scaling. In the gyre portion of the domain, the vertical advection is balanced by vertical diffusion and the thermocline behaves as a diffusive front so that we would expect

$$\delta \sim \left(\frac{\kappa_v f L^2}{\Delta b}\right)^{1/3} \tag{17}$$

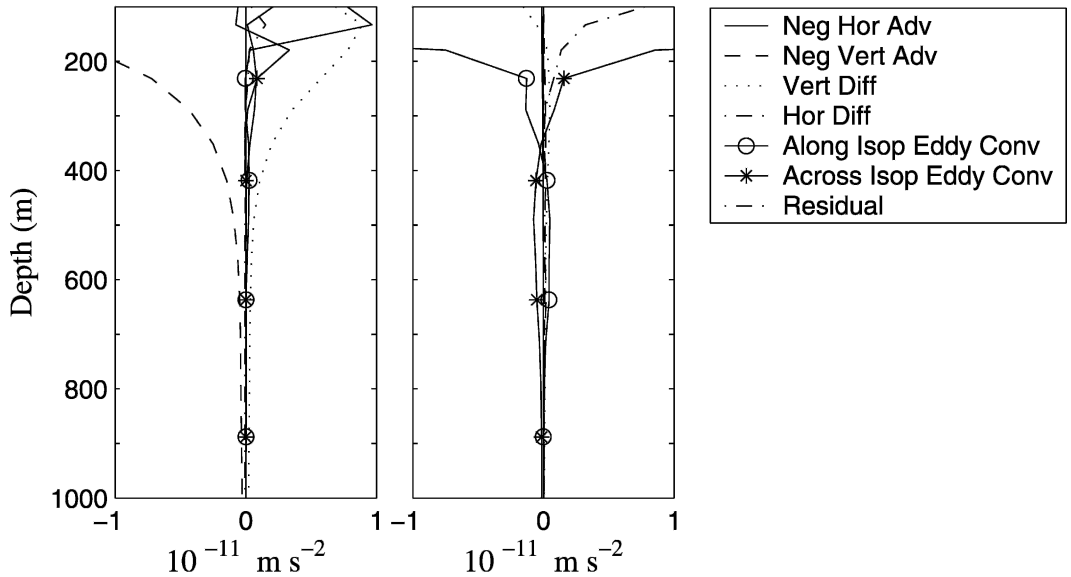

FIG. 11. The terms in the transformed Eulerian mean form of the buoyancy equation for the no-winds case in (left) gyre and (right) channel. The gyre terms are averaged from 6° to 8°E as in Fig. 7, and the channel terms are averaged around the channel.

(Robinson and Stommel 1959; Bryan 1987), where δ represents the total stratification depth, κ_v is the vertical diffusivity, L is the domain scale, and Δb is the surface buoyancy change and is close to the restoring value.

Figure 12 shows a log–log plot of the stratification thickness as a function of κ_v in the eddy-permitting case with no winds. In the channel, this thickness is calculated as the depth of the subsurface maximum in the

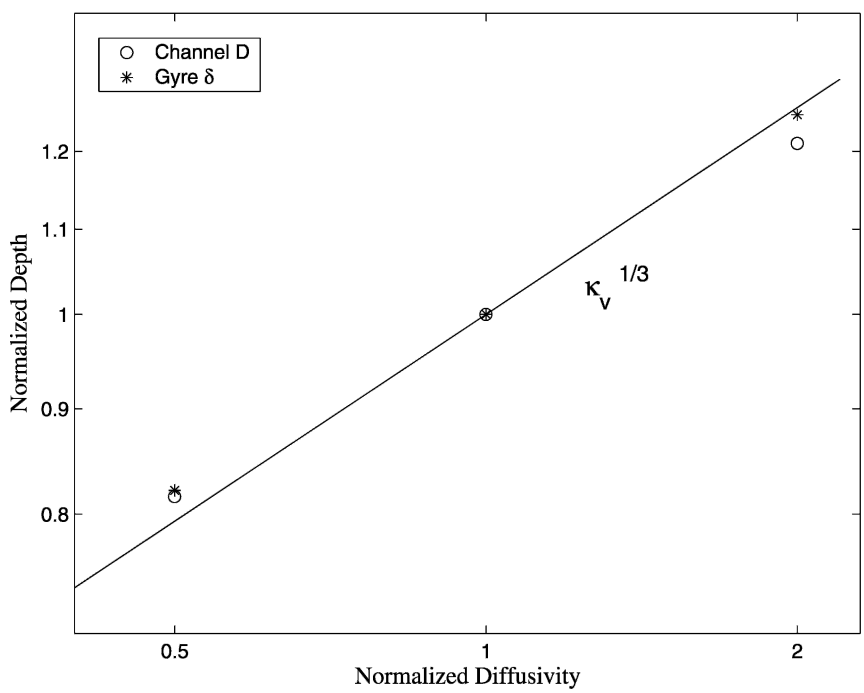

FIG. 12. A log–log plot of the channel stratification depth (circles) and gyre stratification thickness (stars) as a function of the diffusivity in the case with no winds. The diffusivity and depth values have been normalized by their base case values. Also shown is a line whose slope is consistent with a dependence on the diffusivity to the third power. In general, both the channel and gyre depths support a dependence on the diffusivity to the one-third power.

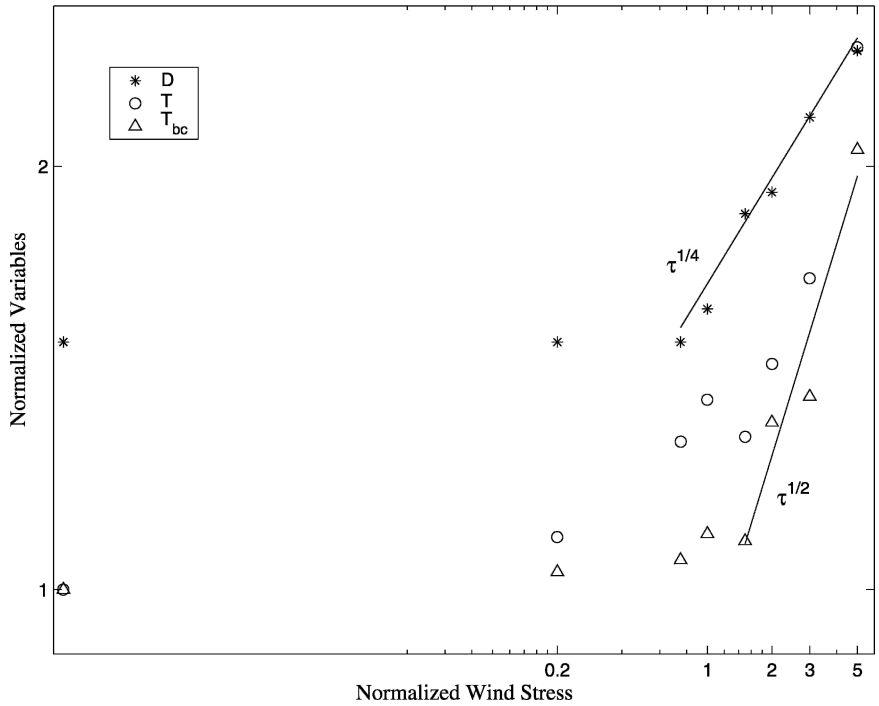

FIG. 13. A log–log plot of the depth of the stratification (stars), the total zonal transport (circles), and the baroclinic transport (triangles) as a function of the wind stress. The variables have been normalized by the no-winds case and the wind stresses are normalized by the base case value. The no-winds case, shown on the left side of the plot, is given a wind stress of 0.000 01 so that it appears on the log plot. Also shown are lines whose slopes are consistent with a dependence on the wind stress to the one-half and one-fourth power.

temperature gradient profile. In the gyre, the depth is defined as the half width of the temperature gradient profile for the isotherms that outcrop in the channel. The thicknesses and diffusivities have been normalized by the case run with $\kappa_v = 2 \times 10^{-5}$ m^2 s^{-1}. In both the channel (circles) and gyre (stars), the thicknesses support the dependence on the diffusivity to the one-third power. In the channel, the explicit diffusion is small, but the stratification depth is still consistent with a diffusive balance, suggesting the eddy diapycnal terms in the channel at least in part owe their existence to the gyre diffusion.

c. *Comparison of the depth scale in the two regimes*

Thus, we have two separate scaling predictions based on different regimes. For low winds, the Ekman transport is small and the eddy circulation must be balanced by the diapycnal processes. This crucial process appears to be the diffusion in the gyre, which deepens the stratification in both the gyre and the channel. This deepening leads to cross-isopycnal eddy fluxes, the convergence of which balances the eddy-driven advection. As the winds increase, the Ekman circulation can balance the eddy circulation, the residual mean decreases, and the channel flow is more adiabatic. Quite coincidentally, it appears the base case (which is the most oceanically relevant case) may represent a transition between these two regimes in the model. In terms of rough magnitudes, using $\kappa_v = 2 \times 10^{-5}$ m^2 s, $f \sim 10^{-4}$ s^{-1}, $L \sim 5 \times 10^6$ m, $\Delta b \sim g\alpha\Delta T$, $g = 9.8$ m s^{-2}, $\alpha \approx 10^{-4}$ K^{-1}, and ΔT for the entire channel + gyre region ~20 K, then $\delta \sim 150$ m, where this number represents the *e*-folding depth of the exponential stratification profile. For the zero-residual-circulation criterion, using (16) and taking the parameters as in the diffusive case, but giving ΔT the appropriate channel value of 5°C and L the channel width scale of 1×10^6 m, and taking $\tau_o \sim \tau/\rho_o$, $\rho_o \approx 1000$ kg m^{-3}, $a = 6.4 \times 10^6$ m, and $\tau = 0.02$ N m^{-2}, then $D \sim 200$ m. These two depth scales are similar in magnitude, lending further support to the idea that both the diffusion and the condition of no net flow compete to set the stratification depth. We now turn to the experimental results found for a variety of wind stresses.

5. Model results for stratification and transport

A total of eight different wind strengths were integrated to near-equilibration, spanning a range from zero winds to 5 times the strength of the base case. We also varied the background diffusion, with a total variation in the diffusion of a factor of 4. Figure 13 shows

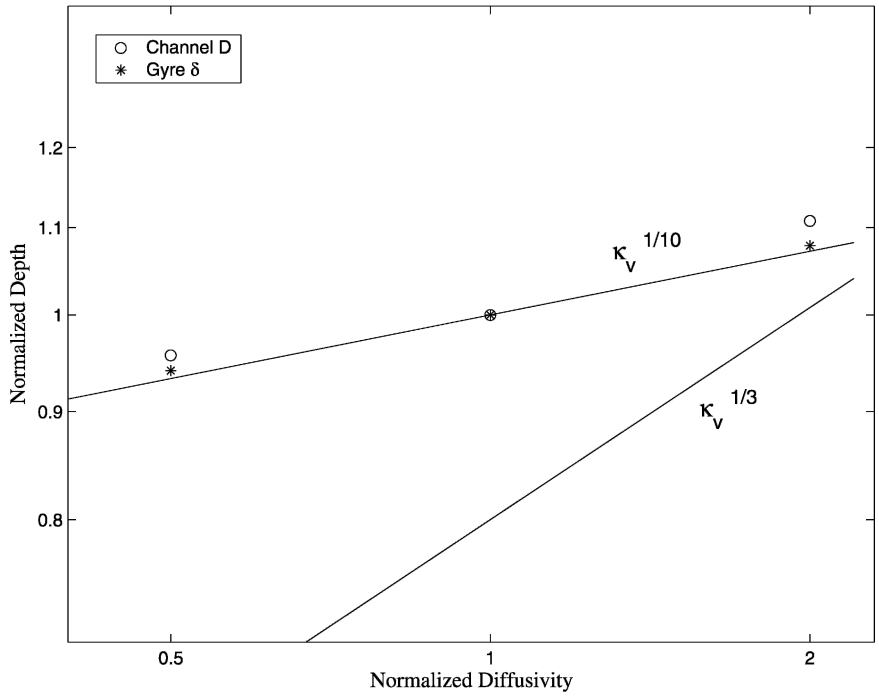

FIG. 14. The same as Fig. 12, but for the base case. Now the depths show little dependence on the diffusivity. Also included is a line whose slope is consistent with a dependence on the diffusivity to the one-tenth power.

how stratification depth and transport change with wind stress. Here, the wind stress is normalized by its base case value and the depth and transport are normalized by the value in the case with no winds. This no-winds case appears on the far left of the figure and is given a nominal value of 0.0001 so that it appears on the log plot. These depths, shown with the stars, show little variation with the wind stress for low wind stress values. However, as the winds are increased beyond the base case value, the depths increase; with the best fit being a dependence on $\tau^{1/4}$. There is some dependence on the wind, although it is somewhat shallower than the $\tau^{2/5}$ prediction derived using zero-residual-circulation theory. The circles in the figure show the overall transport in the channel and the triangles show the baroclinic portion of this transport. According to zonal thermal wind balance, we expect the baroclinic transport, T_{bc}, to go as D^2 since

$$U_{bc} \sim \Delta b D/fL \quad \text{and}$$
$$T_{bc} \sim U_{bc} D,$$

where the first relation comes from thermal wind balance and the second from integrating U_{bc} in the vertical. In the model, the baroclinic transport tends to go as $\tau^{1/2}$, which is consistent with a D^2 dependence. The total transport, which is larger than the baroclinic transport because of a finite barotropic component, also roughly follows a half power dependence, so that the baroclinic and barotropic components increase similarly as the wind increases. This is reasonable, since one expects the barotropic component to form as a result of the convergence of eddy momentum fluxes, and this convergence will likely increase with increasing eddy kinetic energy, which itself increases with increasing wind (not shown).

In the case with no winds, we saw that the gyre internal thermocline thickness and channel stratification depth varied as the diffusivity to the one-third power (Fig. 12). To discover how the stratification depth depends on the diffusivity for larger winds, Fig. 14 shows the stratification depths of cases with base winds but varying diffusivity values. Here, the dependence on the diffusivity is much weaker, showing barely any dependence at all. This suggests the thermocline is no longer strictly in the diffusive regime and that the zero-residual-streamfunction condition is playing a role in setting the stratification depth.

In the base case, the thickness has weak dependence on the gyre diffusion, but the dependence on the wind stress is shallower than the zero-residual-flow condition would imply. This suggests that for moderate to high winds, the model is in a mixed regime, as shown in our revised schematic in Fig. 15. Implicit in this result is the assertion that diffusive processes in the gyre affect the channel stratification. To support this assertion, Fig. 16 shows a plot of the depth of the channel stratification in a simulation with only a channel (circles) as well as the

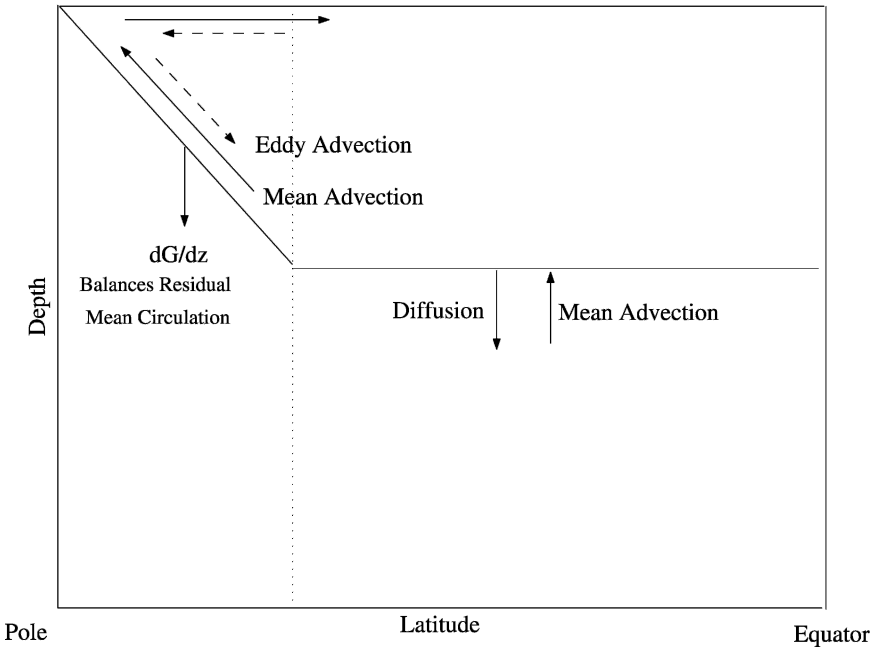

FIG. 15. A revised schematic diagram that takes into account the diapycnal contributions to the buoyancy balance. The mean advection nearly balances the eddy advection in the channel, but the diapycnal eddy flux convergence term also contributes. Also, the diffusion in the gyre plays a role in setting the stratification depth rather than the gyre being a passive region.

case with a channel and a gyre (as in Fig. 13, stars). The channel-only configuration is equal in size to the channel in the base case, but meridionally confined by rigid walls on either side. For reference, the figure includes lines with slope $\tau^{1/4}$ and $\tau^{2/5}$. In the case without a gyre, the stratification changes much more strongly with the wind stress than the case with a gyre. For the no-winds case (far left), the dependence is weaker than the pre-

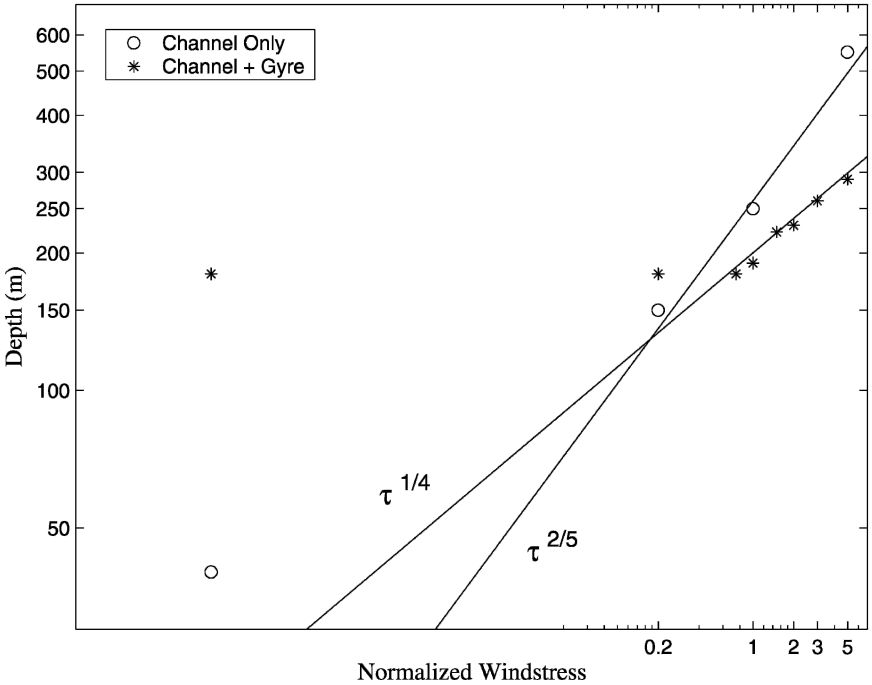

FIG. 16. A log–log plot of the channel stratification depth as a function of the wind stress for the case that only has a channel (circles) and for the base case that includes a channel and a gyre region (stars, as in Fig. 13). Also shown for reference are lines with slope $\tau^{1/4}$ and $\tau^{2/5}$.

dicted $\tau^{2/5}$, but for the other cases tested, the dependence is much closer to the $\tau^{2/5}$ than the channel + gyre base case. Evidently, the gyre dynamics can play an active role in setting the channel stratification and shoal the dependence on the wind stress, although the details of how gyre diffusion leads to channel cross-isopycnal buoyancy fluxes remains only partially understood.

6. Summary and discussion

We have seen that eddies have a pronounced effect on the circulation in a circumpolar current, although in a case with realistic winds and buoyancy forcing, the eddies do not wholly balance the mean circulation. The residual mean remains of moderate strength and tends to be equatorward in the upper ocean and poleward at depth. This picture is broadly consistent with the upper cell described by Speer et al. (2000) in which Upper Circumpolar Deep Water (UCDW) in the Southern Ocean is lifted to the surface and transported out of the channel by the Ekman flux, although a precise comparison is not possible because of the absence of North Atlantic Deep Water and salinity in our model. The exclusion of both NADW and salinity limits the deep cell but likely does not qualitatively change the scalings for the stratification depth.

Depending on the relative strength of the wind and diffusion there are different scaling regimes for the stratification and transport. In a case with weak wind stress but with buoyancy forcing, the channel thermocline depth is largely determined by the vertical diffusion. As winds are increased, both the diapycnal mass fluxes and eddy fluxes together close the Ekman circulation, and in the limit of strong winds the zero residual flow is nearly parallel to the isopycnals. If the mixing length is chosen to be the Rhines scale, then a zero residual flow condition gives a dependence of the stratification depth on the wind stress to the 2/5 power, and a transport dependence of $\tau^{4/5}$. In reality, when the channel is connected to a subtropical gyre, both the diffusion and the zero residual flow condition compete to set the stratification depth (as in Fig. 15), so that the depth depends on the wind stress but with a shallower dependence than the 2/5 power law. However, in a model with only a channel and no gyre, the dependence is much closer to this ideal 2/5 power law. The presence of a gyre, and the presence of more than one scaling regime, likely account for the difference in scaling laws between this study and Gallego et al. (2004) and Karsten et al. (2002), neither of which contain a gyre region. Note that the latter study suggests that transport depends linearly on wind stress, close to our 4/5 prediction.

The real ACC is of course a more complicated system than the model presented here, and due care must be taken in ascribing any but the most robust results of these simulations to that system. The absence of salinity and the simplified geometry (including the lack of a Northern Hemisphere) are the two largest simplifications that we have made. In addition, the residual circulation in a model must be in balance with the surface buoyancy fluxes; in our model, these fluxes are determined by the restoring boundary condition, which may not be realistic and may alter the nature of the residual circulation (Speer et al. 2000). Nevertheless, that mesoscale eddies do greatly influence the stratification and transport seems almost certain, not only from these simulations but from the more realistic FRAM simulations. It also seems likely that both wind stress and thermodynamics (both surface thermodynamic forcing and diapycnal diffusion) affect the transport, although the actual dependence on wind stress and diffusivity can likely only be determined using a more complete model.

Acknowledgments. We thank John Marshall, Timour Radko, Kirk Bryan, Paul Kushner, and two anonymous reviewers for their helpful comments. We also thank John Marshall for providing space and computing resources to CCH. This work was supported in part by the National Science Foundation, and a National Defense Science and Engineering Graduate Fellowship and Clare Luce Fellowship to CCH.

APPENDIX

The Equipartition of Energy and the Channel Scaling Theory for Various Eddy Length Scales

The assumption that the eddy kinetic energy approximately equals the eddy potential energy—an equipartition assumption (Larichev and Held 1995)—relates the eddy length scale to the eddy velocity scale. In this case,

$$\overline{v'^2} \sim \frac{\overline{b'^2}}{N^2} \tag{A1}$$

or

$$\overline{v'^2} \sim \frac{\overline{b}_y^2 L_e^2}{N^2}. \tag{A2}$$

Using $N^2 \sim \Delta b/D$, and solving for U_e,

$$U_e \sim (\Delta b D)^{1/2} \frac{L_e}{L}. \tag{A3}$$

Then, given L_e, this gives the scaling for U_e under equipartition.

a. The radius of deformation

If $L_e \sim L_d$, the deformation radius $[(\Delta b D)^{1/2}/f]$, then U_e is the thermal wind:

$$U_e \sim (\Delta bD)^{1/2} \frac{(\Delta bD)^{1/2}}{fL} \sim \frac{\Delta bD}{fL} \tag{A4}$$

and

$$\kappa_e \sim \frac{(\Delta bD)^{3/2}}{f^2 L}. \tag{A5}$$

Then, using (9),

$$D \sim \left(\frac{\tau_o L^2 f}{\Delta b^{3/2}}\right)^{2/5}. \tag{A6}$$

b. The Rhines scale

If $L_e \sim L_{Rh}$, the Rhines scale $[(U_e/\beta)^{1/2} \sim (U_e a/f)^{1/2}]$, where a is the radius of the earth, then

$$U_e \sim (\Delta bD)^{1/2} \frac{(U_e a)^{1/2}}{f^{1/2} L}, \tag{A7}$$

and solving for U_e gives

$$U_e \sim \frac{\Delta bD}{fL} \frac{a}{L}, \tag{A8}$$

so that in this case, the eddy velocity scales as the thermal wind times the constant a/L. Then,

$$\kappa_e \sim \frac{(\Delta bD)^{3/2}}{f^2 L} \left(\frac{a}{L}\right)^2 \tag{A9}$$

and

$$D \sim \left(\frac{\tau_o L^2 f}{\Delta b^{3/2}}\right)^{2/5} \left(\frac{a}{L}\right)^{4/5}. \tag{A10}$$

c. The domain scale

If $L_e \sim L$, the domain scale, then

$$U_e \sim (\Delta bD)^{1/2} \tag{A11}$$

and

$$\kappa_e \sim (\Delta bD)^{1/2} L. \tag{A12}$$

In our model, we found the eddy length scale to be near the Rhines scale. Alternatively, the Rhines scale could be larger than the domain size, especially for a high-latitude channel (where β is small) and in the presence of high winds (where U_e is large). In that case, the cascade of eddy kinetic energy proceeds all the way to the domain scale, and $L_e \sim L$. The equipartition of energy suggests that

$$U_e \sim (\Delta bD)^{1/2} \frac{L_e}{L}, \tag{A13}$$

so that in the case of $L_e \sim L$, the eddy diffusion, $U_e L_e$, goes as $(\Delta bD)^{1/2}$. Then, the zero residual circulation condition gives

$$D \sim \left(\frac{\tau_o}{f \Delta b^{1/2}}\right)^{2/3}. \tag{A14}$$

If instead we allow U_e to go as the thermal wind, $\Delta bD/fL$, then the zero residual circulation condition gives

$$D \sim \left(\frac{\tau_o L}{\Delta b}\right)^{1/2} \tag{A15}$$

as used in Karsten et al. (2002).

REFERENCES

Andrews, D. G., and M. E. McIntyre, 1978: An exact theory of nonlinear waves on a Lagrangian-mean flow. *J. Fluid Mech.,* **89,** 609–646.

Bryan, F. O., 1987: Parameter sensitivity of primitive equation ocean general circulation models. *J. Phys. Oceanogr.,* **17,** 970–985.

Doos, K., and D. J. Webb, 1994: The Deacon cell and other meridional cells of the Southern Ocean. *J. Phys. Oceanogr.,* **24,** 429–442.

Gallego, B., P. Cessi, and J. C. McWilliams, 2004: Antarctic Circumpolar Current in equilibrium. *J. Phys. Oceanogr.,* **34,** 1571–1587.

Gent, P. R., J. Willebrand, T. McDougall, and J. C. McWilliams, 1995: Parameterizing eddy-induced tracer transports in ocean circulation. *J. Phys. Oceanogr.,* **25,** 463–474.

Gille, S. T., and R. E. Davis, 1999: The influence of mesoscale eddies on coarsely resolved density: An examination of subgrid-scale parameterization. *J. Phys. Oceanogr.,* **29,** 1109–1123.

Gnanadesikan, A., and R. W. Hallberg, 2000: On the relationship of the Circumpolar Current to Southern Hemisphere winds in coarse-resolution ocean models. *J. Phys. Oceanogr.,* **30,** 2013–2034.

Henning, C. C., and G. K. Vallis, 2004: The effects of mesoscale eddies on the main subtropical thermocline. *J. Phys. Oceanogr.,* **34,** 2428–2443.

Johnson, G. C., and H. Bryden, 1989: On the strength of the circumpolar current. *Deep-Sea Res.,* **36,** 39–53.

Karsten, R. H., and J. Marshall, 2002: Constructing the residual circulation of the ACC from observations. *J. Phys. Oceanogr.,* **32,** 3315–3327.

——, H. Jones, and J. Marshall, 2002: The role of eddy transfer in setting the stratification and transport of a Circumpolar Current. *J. Phys. Oceanogr.,* **32,** 39–54.

Killworth, P. D., and M. M. Nanneh, 1994: Isopycnal momentum budget of the Antarctic Circumpolar Current in the Fine Resolution Antarctic Model. *J. Phys. Oceanogr.,* **24,** 1201–1223.

Larichev, V. D., and I. M. Held, 1995: Eddy amplitudes and fluxes in a homogeneous model of fully developed baroclinic instability. *J. Phys. Oceanogr.,* **25,** 2285–2297.

Marshall, J., and T. Radko, 2003: Residual-mean solutions for the Antarctic Circumpolar Current and its associated overturning circulation. *J. Phys. Oceanogr.,* **33,** 2341–2354.

——, D. Olbers, H. Ross, and D. Wolf-Gladrow, 1993: Potential vorticity constraints on the dynamics and hydrography of the Southern Ocean. *J. Phys. Oceanogr.,* **23,** 465–487.

McIntosh, P. C., and T. J. McDougall, 1996: Isopycnal averaging and the residual mean circulation. *J. Phys. Oceanogr.,* **26,** 1655–1660.

Pacanowski, R. C., and S. M. Griffies, 1999: The MOM 3 manual, alpha version. NOAA/Geophysical Fluid Dynamics Laboratory, 580 pp.

Radko, T., and J. Marshall, 2004: Eddy-induced diapycnal fluxes and their role in the maintenance of the thermocline. *J. Phys. Oceanogr.,* **34,** 372–383.

Rhines, P. B., 1975: Waves and turbulence on a beta-plane. *J. Fluid Mech.,* **69,** 417–443.

Robinson, A., and H. Stommel, 1959: The oceanic thermocline and the associated thermohaline circulation. *Tellus,* **11,** 295–308.

Samelson, R. M., and G. K. Vallis, 1997: Large-scale circulation with small diapycnal diffusion: The two-thermocline limit. *J. Mar. Res.,* **55,** 223–275.

Speer, K., S. R. Rintoul, and B. Sloyan, 2000: The diabatic Deacon cell. *J. Phys. Oceanogr.,* **30,** 3212–3222.

Stommel, H., and J. Webster, 1962: Some properties of the thermocline equations in a subtropical gyre. *J. Mar. Res.,* **44,** 695–711.

Straub, D. N., 1993: On the transport and angular momentum balance of channel models of the Antarctic Circumpolar Current. *J. Phys. Oceanogr.,* **23,** 776–782.

Vallis, G. K., 2000: Large-scale circulation and production of stratification: Effects of wind, geometry, and diffusion. *J. Phys. Oceanogr.,* **30,** 933–954.

——, and M. E. Maltrud, 1993: Generation of mean flows and jets on a beta plane and over topography. *J. Phys. Oceanogr.,* **23,** 1346–1362.

Welander, P., 1959: An advective model of the ocean thermocline. *Tellus,* **11,** 309–318.

Wilkin, J. L., and R. A. Morrow, 1994: Eddy kinetic energy and momentum flux in the Southern Ocean: Comparison of a global eddy-resolving model with altimeter, drifter, and current-meter data. *J. Geophys. Res.,* **99** (C4), 7903–7916.